Dalton Transactions

Energy transfer phenomena and colour tunability in Y2O2S:Eu3+/Dy3+ micro-fibers for white emission in solid state lighting application

Journal:	*Dalton Transactions*
Manuscript ID:	DT-ART-02-2014-000349.R1
Article Type:	Paper
Date Submitted by the Author:	20-Feb-2014

Complete List of Authors:	Som, Sudipta; University of The Free State, Department of Physics Mitra, Priyanka; Indian School of Mines, Department of Applied Physics Kumar, Vijay; University of the Free State, P.O. Box 339, Bloemfontein 9300, Republic of South Africa , Physics Kumar, V; University of the Free State, Department of Physics Terblans, Jacobus; University of the Free State, Department of Physics Swart, Hendrik; University of the Free State, Department of Physics Sharma, Shailendra; Indian School of Mines, Department of Applied Physics

Energy transfer phenomena and colour tunability in $Y_2O_2S:Eu^{3+}/Dy^{3+}$ micro-fibers for white emission in solid state lighting application

S. Som [a,b,], P. Mitra [b], Vijay Kumar [a], Vinod Kumar [a], J. J. Terblans [a], H. C. Swart[a], S. K. Sharma [b, *]*

[a]Department of Physics, University of Free State, P.O. Box 339, Bloemfontein, ZA 9300, South Africa

[b]Department of Applied Physics, Indian School of Mines, Dhanbad 826004, India

Tel.: +27 514013852/ +27 58 718 5308;

Fax: +27 58 718 444.

[*]Corresponding author E Mail: sudipta.som@gmail.com (S Som)

sksharma.ism@gmail.com (S K Sharma)

KEYWORDS**:** phosphor; energy transfer; solid state lighting; $Y_2O_2S: Eu^{3+}/ Dy^{3+}$.

ABSTRACT: This paper reports on the structural, optical and photometric characterization of Eu^{3+}/ Dy^{3+} doped yttrium oxysulfide phosphor (Y_2O_2S: Eu^{3+}/ Dy^{3+}) for near white emission in solid state lighting. A series of Y_2O_2S phosphors doped with Eu^{3+}/ Dy^{3+} were prepared by hydrothermal method. The microstructures of the as-synthesized phosphors were investigated by X-ray diffraction (XRD) and Scanning electron microscopy (SEM). The XRD results reveal that the obtained powder phosphors are single-phase hexagonal structure and also indicate that the incorporation of the dopants/ co-dopants did not affect the crystal structure. The SEM images reveal the morphology of the prepared phosphors as an intense interpenetrating network of interconnected micro-fibers of diameter of about 0.15 μm. The band gap of the phosphors was calculated from diffuse reflectance spectra using the Kubelka-Munk function. The Eu^{3+}, Dy^{3+} doped and Eu^{3+}/ Dy^{3+} co-doped phosphors illuminated with ultraviolet light showed the characteristic red luminescence corresponding to the $^5D_0 \rightarrow {}^7F_J$ transitions of Eu^{3+} and the characteristics blue and yellow luminescence corresponding to the $^4F_{9/2} \rightarrow {}^6H_{15/2}$ or $^4F_{9/2} \rightarrow {}^6H_{13/2}$ transitions of Dy^{3+}. The luminescence spectra, the energy transfer efficiency and decay curves of the phosphors indicated that there exists a strong energy transfer from Dy^{3+} to Eu^{3+} and which was demonstrated to be a resonant type via a dipole-quadrupole reaction. Furthermore, the critical distance of the Eu^{3+} and Dy^{3+} ions has also been calculated. By utilizing the principle of energy transfer, it was also demonstrated that with an appropriate tuning of the activator content the Y_2O_2S: Eu^{3+}/ Dy^{3+} phosphors exhibit a great potential to act as a single- emitting component phosphors for white light emission in solid state lighting technology.

INTRODUCTION

The research efforts to fabricate effective new phosphor materials for the application in next-generation displays and solid state lighting have been the subject of intense research during

the last decades.[1-5] In recent years, white light emission from single emitting component phosphors have attracted much attention due to their low electric consumption, high brightness and colour quality and less complex characteristics.[6-8] Hence, there is growing interest in developing white light emitting phosphors for applications in display and lighting. The white-light can be achieved through the combination with the recently available blue, green, and red phosphors according to the appropriate ratio.[9-10] However, this method is hard to work in practice since different emitting components require different drive voltages and one can hardly be sure about the consistency in the decay process for the different components, thus resulting in the change in color with time and the complex behavior of the circuit.[6, 9-10] A more feasible approach is to find such a material that can produce white-light emission via the combination of different color emission from an identical luminescence center.[9] Recently, a lot of research works have been carried out to develop the single-phased white-emitting phosphors which are based on the mechanism of the energy transfer from sensitizer to the activator, such as Tb^{3+}/Dy^{3+}[11] and Ce^{3+}/Dy^{3+}[1, 12] for white light applications. Dy^{3+} doped luminescent materials have been known to exhibit, two principal emissions in the blue and yellow regions corresponding to the $^4F_{9/2}\rightarrow{}^6H_{15/2}$ and $^4F_{9/2}\rightarrow{}^6H_{13/2}$ transitions. By adjusting the yellow-to-blue intensity ratio (Y/B) appropriately, it is possible to obtain pure white light from Dy^{3+} activated luminescent materials.[6] Owing to the forbidden f–f transitions of Dy^{3+} ions and low absorption cross-section ($\sim$0.01–1cm^{-1}) the emission intensity of Dy^{3+} singly doped phosphor is poor under UV excitation.[6] Moreover, the quality of white light emission from Dy^{3+} activated luminescent materials is poor due to the lack of the red light component.[6] This necessitates the codoping of some red emitting materials in Dy^{3+} doped phosphors. It is well known that Eu^{3+} is a popular activator ion for many different host lattices for a rich red emission.[12] Dy^{3+} ions are usually introduced into Eu^{3+} doped luminescence materials to enforce the Eu^{3+} emission. Combining this red emission with Dy^{3+}

emission it is possible to achieve white light with good quality. But for this to happen, a good host also is required. Yttrium oxysulfide has long been known as an excellent host material for tunable colour emitting phosphors.[13] Manashirov et al. developed and commercialized yttrium oxysulfide based blue, yellow and green phosphors and achieved white light from a triply doped complex oxysulfide system.[14] A white long-lasting phosphor based on Y_2O_2S: Tb^{3+}, Sm^{3+} is reported by Lin Lin et al. [15] However, the studies on the energy transfer (ET) process between the Eu^{3+} and Dy^{3+} pair is rarely reported. No work has been reported on the white light emission from Y_2O_2S: Eu^{3+}/ Dy^{3+} single emitting phosphor component on the basis of energy transfer (ET). Therefore, a considerable interest has been grown to dope and co-dope Y_2O_2S phosphors by Eu^{3+} and Dy^{3+} ions. The luminescent behavior and the ET phenomenon of doped and co-doped Eu^{3+} and Dy^{3+} in Y_2O_2S phosphors are discussed.

EXPERIMENTAL DETAILS

Synthesis of rare-earth doped/ co-doped yttrium oxysulfide phosphors. Eu^{3+} doped, Dy^{3+} doped and Eu^{3+}/ Dy^{3+} co-doped Y_2O_2S phosphor were prepared by hydrothermal process followed by solid state reaction.[16] In the synthesis method europium oxide (Eu_2O_3), dysprosium oxide (Dy_2O_3), yttrium oxide (Y_2O_3), nitric acid (HNO_3), sodium carbonate (Na_2CO_3) and sodium thiosulfate ($Na_2S_2O_3$, $5H_2O$) were used as starting ingredients. The stock solutions of $Y(NO_3)_3$, $Eu(NO_3)_3$ and $Dy(NO_3)_3$ were prepared by dissolving Y_2O_3, Eu_2O_3 and Dy_2O_3 in nitric acid and diluting with deionized water. The Dy doped samples were prepared by mixing $Y(NO_3)_3$ and $Dy(NO_3)_3$ according to the formula $Y_{2-x}Dy_xO_2S$ (x = 0.02, 0.04, 0.06, 0.08, 0.10). Similarly, Eu doped samples were prepared by mixing $Y(NO_3)_3$ and $Eu(NO_3)_3$ according to the formula $Y_{2-y}Eu_yO_2S$ (y = 0.02, 0.06, 0.10, 0.14, 0.20). The Eu, Dy co-doped samples were prepared by mixing $Y(NO_3)_3$, $Eu(NO_3)_3$ and $Dy(NO_3)_3$ according to the formula $Y_{2-y-x}Eu_yDy_xO_2S$ and varying the x/y ratio. NaOH was introduced drop-wise to

the vigorously stirred mixed nitrate solution until the pH of the mixed solution was observed between 9 to10. The obtained white precipitate then transferred to a 100 mL Teflon-lined stainless steel autoclave and heated at 200°C for 14 hours. The autoclave was then naturally cooled at room temperature.[6] The resultant precursor was washed several times with deionized water and absolute ethanol, and then dried at 70°C for 5 hours. The sulphurization of the prepared precursor was performed by solid state reaction using the concept of topotactic reaction.[16] In topotactic reaction morphology of the material does not change while the phase of the material changes. Sodium carbonate (Na_2CO_3) and Sodium-thiosulphate ($Na_2S_2O_3.5H_2O$) were mixed and pulverized with the obtained precursor in a mortar pestle. This mixture was then calcined at a temperature of 1200°C for 1 hour. During heating, the crystalline lattice of the Y_2O_3 precursor is sulphureted yielding the Y_2O_2S phosphor. The high temperature synthesis reaction is: [17-18]

$$(5\text{-}x)\ Na_2CO_3 + (3x+1)\ Na_2S_2O_3 \rightarrow 2(x+1)\ Na_2SO_4 + 4Na_2S_x + (5\text{-}x)\ CO_2$$

$$Y_2O_3 + Na_2S_x \rightarrow Y_2O_2S + \tfrac{1}{2}\ O_2 + Na_2S_{x-1} \qquad (1)$$

After cooling, the reaction product was washed a few times with water to remove the residual flux (Na_2CO_3) and the desired phosphor was obtained. During the synthesis, sodium thiosulphate was used to achieve the sulphuration of Y_2O_3 and sodium carbonate was used as flux.[18]

Characterization of rare-earth doped/ co-doped yttrium oxysulfide phosphors. X-ray diffractogram of prepared phosphors were recorded in a wide range of Bragg angles 2θ ($20° \leq 2\theta \leq 90°$) using a Bruker D8 advanced X-ray diffraction (XRD) measuring instrument with Cu target radiation ($\lambda = 0.154056$ nm). Scanning electron microscope (SEM) images were obtained using a Shimadzu SSX-550 Superscan SEM at different magnification to examine the crystallinity and surface morphology of the prepared phosphors. The diffuse reflectance

(DR) spectra were recorded using a Perkin-Elmer make Lambda 35 UV–VIS spectrophotometer in the wavelength range 200-800 nm. The photoluminescence (PL) studies were carried out on a Hitachi Fluorescence Spectrometer F-2500 with a 150W Xe lamp as an excitation sources in the range 220-650 nm. The decay kinetics was studied on a Quanta Master 40 fluorometer. All the studies were carried out at room temperature.

RESULT AND DISCUSSION

Phase identification and morphology. Figure 1 shows the XRD patterns of undoped, Eu^{3+}, Dy^{3+} (3 mol%) doped and Eu^{3+}/Dy^{3+} (3:3) co-doped Y_2O_2S phosphors. The XRD peaks of undoped phosphor were identified and indexed according to the JCPDS file No. 24-1424.[19] The sharp and single diffraction peaks of the XRD pattern confirm the formation of a single phase compound. The (hkl) values were labeled on the peaks. This implies that the Y_2O_2S phosphors have a hexagonal structure with space group $P\bar{3}m1$ and lattice constant a=b= 3.784 Å, c = 6.589 Å; α=β= 90º and γ=120º. No new peaks were observed in the XRD patterns after doping and codoping, which indicates that the incorporation of Eu^{3+} and Dy^{3+} into the Y_2O_2S lattice did not induce any significant changes in the structure of the host material.[20]

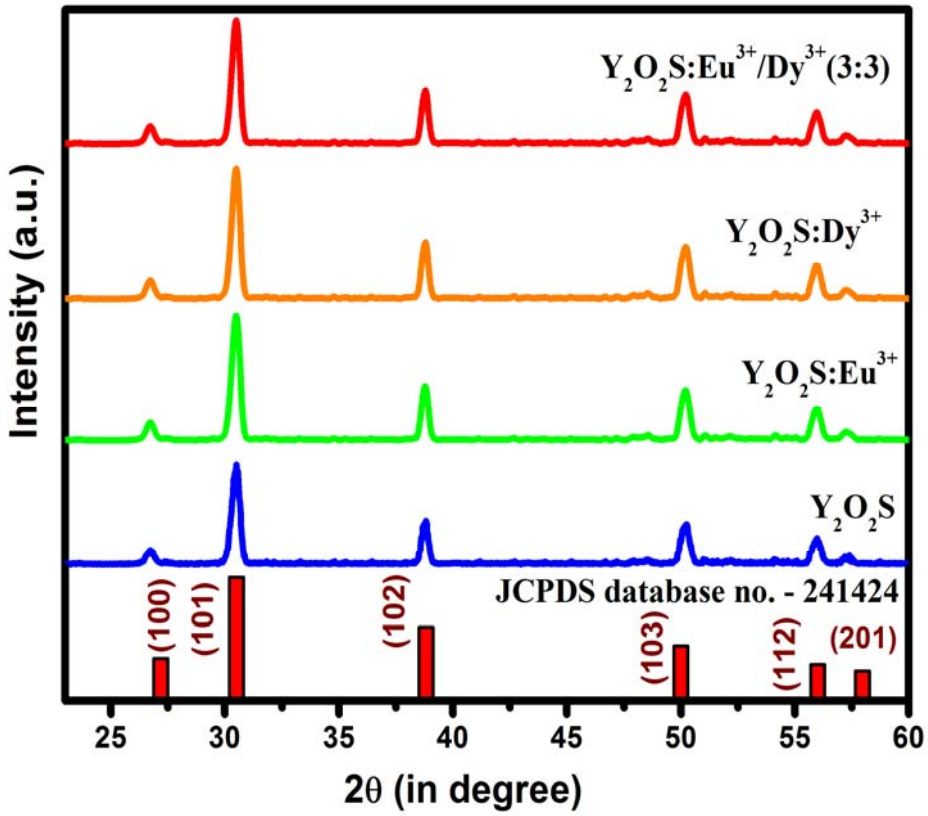

Fig. 1: *XRD patterns of undoped, doped and co-doped Y_2O_2S phosphors.*

To obtain the information about the morphology, grain size and shape of the synthesized phosphor, SEM studies were carried out for the undoped and co-doped Y_2O_2S phosphors. Fig.2. shows the SEM micrograph of the undoped Y_2O_2S (Fig. 2 a) and the $Y_{1.94}Eu_{0.03}Dy_{0.03}O_2S$ (Fig. 2 b) with different magnifications, as indicated. The SEM images show that the Y_2O_2S consist of interconnected micro-fibers of diameter of about 0.15 μm, which forms an intense interpenetrating core-spike network.[21] The rough surface of the Y_2O_2S might also be very useful for light harvesting due to the high surface to volume ratio.[21- 24]

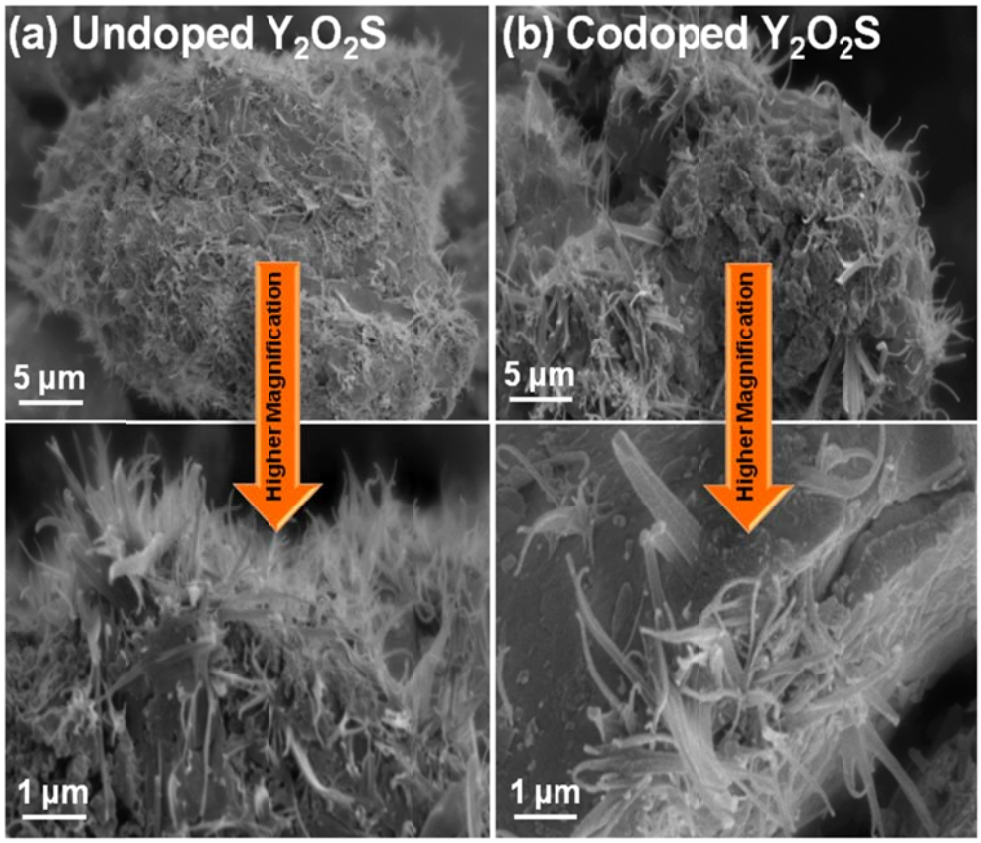

Fig. 2: *SEM images of Y_2O_2S phosphors.*

The diameter for the fiber shaped particles were found to obey the log normal nature[25]

$$P(d) = \frac{1}{d\sigma\sqrt{2\pi}} exp[\frac{-ln^2(d/\bar{d})}{2\sigma^2}] \quad (2)$$

Here d and σ are related to the average size and the size distribution of the particles. And it was found that the average diameter of undoped phosphor was estimated to be 0.15 µm with a narrow size distribution (σ=0.20) and of co-doped phosphor was estimated to be 0.17 µm with a relatively wider size distribution (σ=0.25). There is a very little difference in the SEM morphology and average diameter of undoped and codoped Y_2O_2S indicating that doping/ codoping does not affect the structure and morphology of the synthesized phosphors.[26]

The mechanism for the formation of the fibrous morphology normally involves two steps, one is the nucleation and growth of particles and the second is self-assembly by oriented

attachments.[27] The assembly of the particles in a certain way is the main initiation step for the formation of the fiber. The synthesized and growth mechanism in this case may be summarized as follows: all the reactants were dissolved in the aqueous solution under intensive stirring and the pH was kept between 9 to 10 as shown in Fig. 3 (a). A flocculent type precipitates (Fig. 3 (b)) was observed after dissolving the reactants in the aqueous solution. This suspension was transferred into a Teflon-lined stainless steel autoclave. The autoclave was maintained at a fixed temperature of 200°C for 14 h without stirring or shaking. In this hydrothermal condition, nuclei were formed from the flocculent precipitates in the suspension as shown in Fig. 3 (c). Then the nuclei start to grow by consuming the flocculent precipitates materials (Fig. 3 (d)). Due to the electrostatic gravitation and intermolecular force, the larger nanoparticles fell to the bottom of the autoclave and start to aggregate the particles (Fig. 3 (e)). The smaller ones were attached to the aggregate and can coalesce under hydrothermal conditions in oriented attachment extended in a certain way (Fig. 3 (f)). [28] This is because of the anisotropic growth of the nanocrystals in a template-free method. It is generally related to the different surface energies of different crystal planes of the nanocrystals. These planes with high surface energy have a strong tendency to capture smaller nanoparticles from the reaction solution in order to reduce their surface energy. This leads to growth along those almost perfectly aligned crystalline lattice planes and formation of the 1D fibrous morphology as shown in Fig. 3 (g) .[27-29] The resultant precursor was washed several times with deionized water and absolute ethanol, and then dried at 70 °C for 5 hours. The sulphurization of the prepared fibre bundles was performed by solid state reaction using the concept of topotactic reaction.[16]

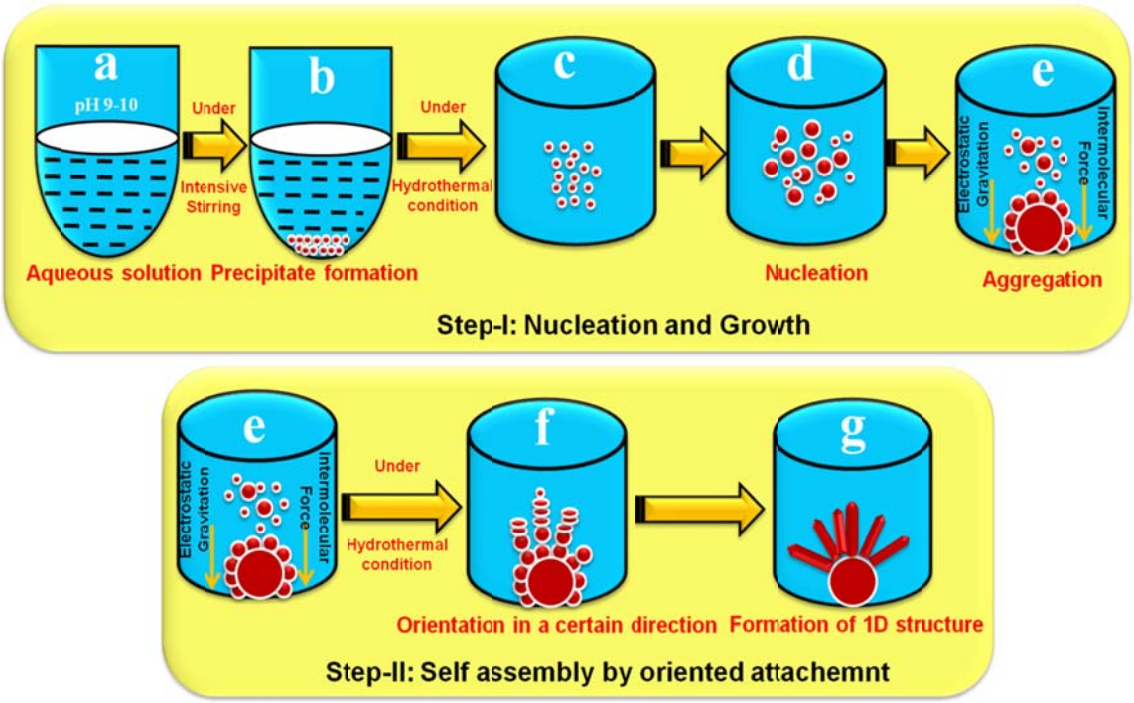

Fig. 3: Schematic diagram for the formation of fibrous morphology.

Diffuse reflectance spectroscopy and bandgap. The DR spectra of undoped, doped and co-doped Y_2O_2S phosphors were measured against a reference standard spectralon compound. In diffuse reflectance spectra, a sharp band at 213 nm was observed for all samples as shown in Fig. 4. The band at 213 nm was due to the band gap of the undoped, doped and co-doped Y_2O_2S phosphors. In case of the Y_2O_2S: Eu^{3+} phosphor a band edge was observed at 250 nm. This is due to the charge transfer from Eu^{3+} to O^{2-}. The other weak bands beyond 300 nm were also observed in the case of doped and co-doped samples. These bands were due to meta-stable energy states formed between the valence band and the conduction band by the RE^{3+} ions.[30] These extra bands were absent in the undoped phosphor. The Kubelka-Munk theory[31] was used to calculate the band gap of undoped, doped and co-doped Y_2O_2S phosphors using DR spectra. In a DR spectra, the ratio of the light scattered from a thick layer of sample and an ideal non-absorbing reference sample is measured as a function of the wavelength λ , $R_\infty = R_{sample} / R_{reference}$.[32] The relation between the diffuse reflectance of the

sample (R_∞), absorption coefficient (K) and scattering coefficient (S) is given by the Kubelka-Munk function $F(R_\infty)$:

$$F(R_\infty) = \frac{(1 - R_\infty)^2}{2R_\infty} = \frac{K}{S} \quad (3)$$

The band gap E_g and linear absorption coefficient α of a material is related through the well-known Tauc relation: [33]

$$\alpha h\nu = C_1(h\nu - E_g)^{n/2} \quad (4)$$

where ν is the photon energy and C_1 is a proportionality constant. When the material scatters in perfectly diffuse manner (or when it is illuminated at 60° incidence), the absorption coefficient K becomes equal to 2α. Considering the scattering coefficient S as constant with respect to wavelength, and using Equations 3 and 4, the following expression can be written:

$$[F(R_\infty)h\nu]^2 = C_2(h\nu - E_g)^n \quad (5)$$

The value of n is 1 for direct allowed transitions, 2 for non-metallic materials, 3 for direct forbidden transitions, 4 for indirect allowed transition and 6 for indirect forbidden transition. Now, among the plot of $[F(R_\infty)h\nu]^2$, $[F(R_\infty)h\nu]$, $[F(R_\infty)h\nu]^{2/3}$, $[F(R_\infty)h\nu]^{1/2}$, $[F(R_\infty)h\nu]^{1/3}$ as a function of photon energy hν, the best fitting was obtained with n = 1 in eq. (5), i.e, $[F(R_\infty)h\nu]^2$ as a function of hν indicating that the band transitions occurred were direct in nature, as suggested by Tauc et al.[32- 33] From the plot of $[F(R_\infty)h\nu]^2$ versus hν, the value of E_g was obtained by extrapolating the linear fitted regions to $[F(R_\infty)h\nu]^2 = 0$.

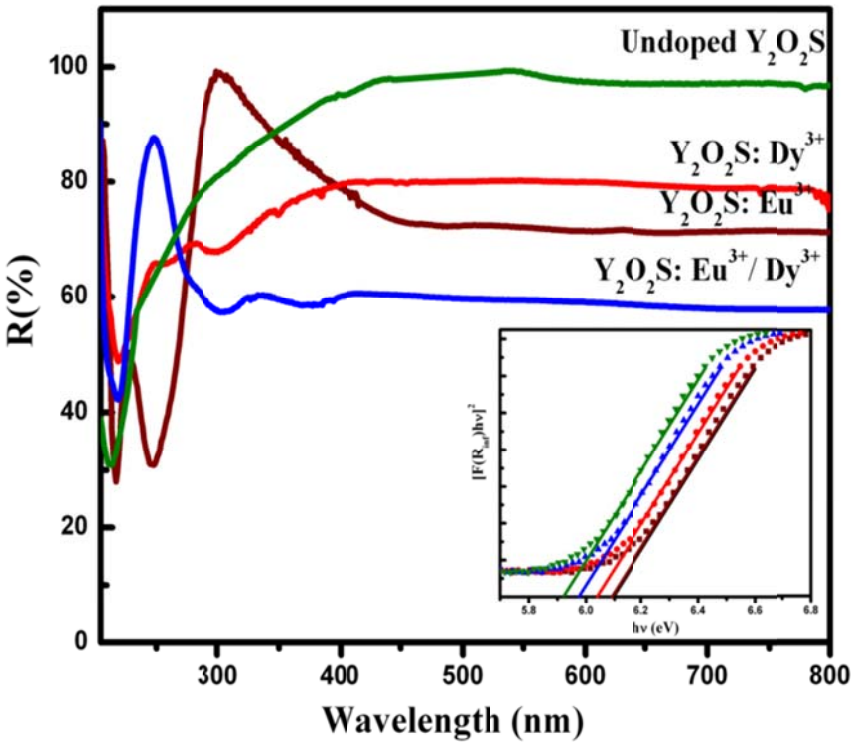

Fig.4: *DR spectra of undoped, doped and co-doped Y_2O_2S phosphors.*

The band gap calculated from the DR spectra using K-M function $F(R_\infty)$ was found to be around 5.91 eV for the undoped, 6.1 and 6.05 eV for Eu^{3+} and Dy^{3+} doped respectively and 5.98 eV for co-doped samples and shown in the inset of Fig. 4.

Photoluminescence spectroscopy and assymmetric ratio. Fig. 5 (a) shows the photoluminescence excitation (PLE) and photoluminescence emission (PL) spectra of Eu^{3+} doped Y_2O_2S phosphor. The PLE spectrum monitored at 614 nm exhibits a wide band from 220-550 nm with maximum intensity at 254 nm, which is assigned to the transitions due to the charge transfer band (CTB) from O^{2-} - Eu^{3+}. Another weak CTB peak ~ 315 nm is observed due to the $Eu^{3+} \leftarrow S^{2-}$ transition.[34] In addition to the 254 and 315 nm peak; three more peaks have also been identified at 394 nm, 466 nm and 533 nm due to absorption of the incident radiation by the Eu^{3+} ions and lead to the excitation of electrons from the Eu^{3+} ground state to its excited 4f levels for the intra-configurational 4f-4f transition of Eu^{3+} in the

host lattice i.e., $^7F_0 \rightarrow {}^5L_6$, $^7F_0 \rightarrow {}^5D_2$ and $^7F_0 \rightarrow {}^5D_1$ transitions respectively.[33] This indicates that these phosphors could be excited both by the near-UV light at 394 nm and blue light at 466 nm, green light at 533 nm along with the CTB, which might found applications in solid-state lighting technology.[12] The similarity in the location and shape of Eu^{3+} emission lines of this phosphor was observed when excited with ~ 254, 394, 466, 533 nm excitation wavelengths excluding their relative intensity.[35] For this reason, the emission spectrum of this Eu^{3+}doped phosphor recorded at an excitation wavelength of 254 nm is depicted alone in Fig. 5(a). It exhibits distinct emission lines in between 500 - 700 nm with strongest emission at 614 nm. These emission lines were observed due to transitions form excited $^5D_1$ to $^7F_1$ and $^5D_0$ to ^7F_j (j = 0-4) levels of Eu^{3+} ions.[20] Most intense peaks at 614 and 631 nm correspond to the hypersensitive transition $^5D_0 \rightarrow {}^7F_2$ levels of the Eu^{3+} ion due to the forced electric dipole transition mechanism. The weak emission in the vicinity of 591 nm (590-600 nm) is ascribed to the magnetic dipole transition of $^5D_0$ to $^7F_1$. It is well known that $^5D_0 \rightarrow {}^7F_2$ hypersensitive transition is strongly influenced by the outside surroundings. When the Eu^{3+} is located at a low symmetry local site, this emission transition is often dominated in their emission spectra. The performance of luminescent materials is influenced by the doping concentration and it is very important to determine the optimum concentration for luminescence application.[20] Emission spectra for different Eu^{3+} concentrations (1 mol% -10 mol %) excited at 254 nm are shown in Fig. 5 (b). The PL emission intensity of Y_2O_2S: Eu^{3+} increased with an increase of the Eu^{3+} concentration up to 5 mol% and then decreased due to the concentration quenching phenomena as per the following cross-relaxation mechanism: [20]

$$Eu^{3+}\ (^5D_1) + Eu^{3+}\ (^7F_0) \rightarrow Eu^{3+}\ (^5D_0) + Eu^{3+}\ (^7F_1)$$

It was reported that the ratio between the integrated intensity of the transitions $^5D_0 \rightarrow {}^7F_2$ and the $^5D_0 \rightarrow {}^7F_1$, known as asymmetric ratio (R/O) [12], can be used as a local crystal field probe

to measure the nature of the local Eu^{3+} surroundings. Thus this ratio indicates the degree of distortion from the inversion symmetry of the Eu^{3+} ion local environment. The emissions of Eu^{3+} will also contain some emission component from the upper excited levels of Eu^{3+}, but compared with the emissions of $^5D_0 \rightarrow {}^7F_2$ and $^5D_0 \rightarrow {}^7F_1$ of Eu^{3+} these contributions are very small, and would not greatly affect the trends of the R/O of Eu^{3+}. The calculated asymmetric ratios were 6.50, 6.58, 6.62, 6.52 and 6.45 for 1, 3, 5, 7 and 10 mol% of doped Eu^{3+} concentrations, respectively, which is strong evidence that Eu^{3+} ions mainly occupy the lattice site without inversion symmetry.[20]

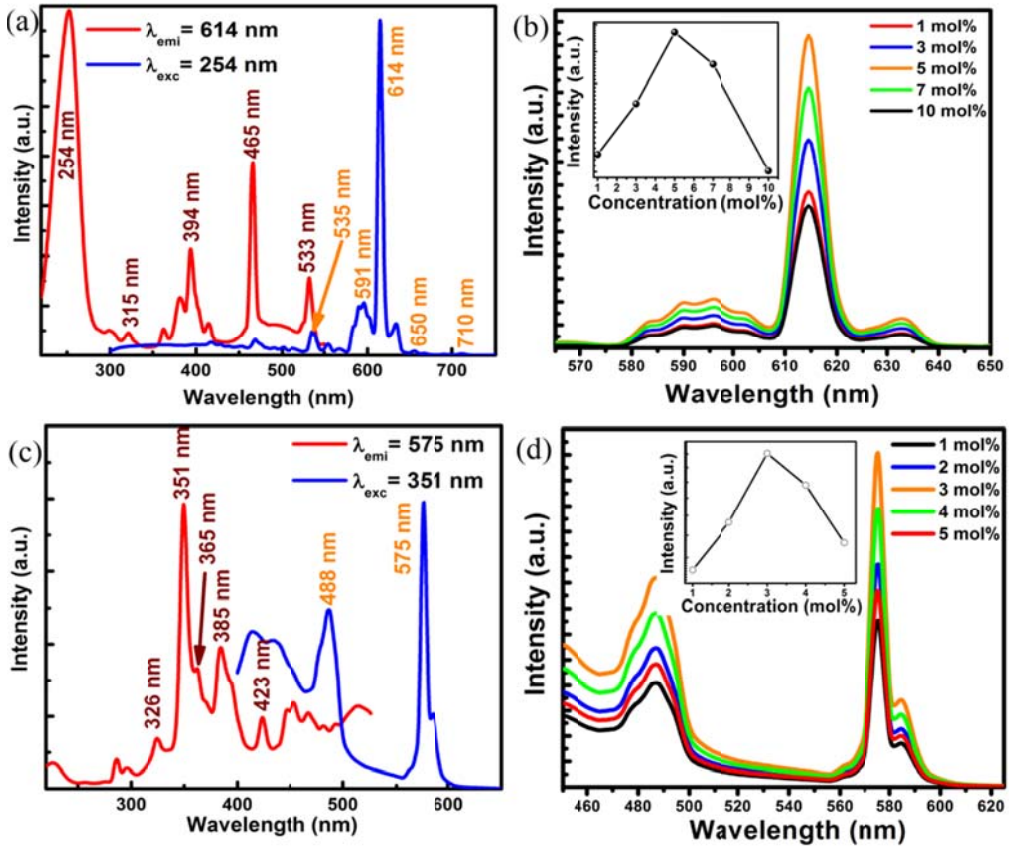

Fig. 5: (a) *PL emission and excitation spectrum for Eu^{3+} doped phosphor* ***(b)*** *variation of PL intensity with Eu^{3+}concentration* **(c)** *PL emission and excitation spectrum for Dy^{3+} doped phosphor* ***(d)*** *variation of PL intensity with Dy^{3+}concentration*

The PLE and PL spectra of Dy^{3+} doped Y_2O_2S phosphor are presented in Fig. 5 (c). The emission spectrum of Dy^{3+} doped phosphor was recorded at an excitation wavelength of 351 nm. It consists of two distinct peaks at 488 and 575 nm corresponding to the $^4F_{9/2} \rightarrow {}^6H_{15/2}$ and $^6H_{13/2}$ transitions, respectively. The 351 nm radiation excites the Dy^{3+} ions to the $^6P_{7/2}$ level and then quickly relaxes to the $^4F_{9/2}$ level by emitting non-radiative transitions. The strong yellow emission band centered at 575 nm corresponds to the hypersensitive transition $^4F_{9/2} \rightarrow {}^6H_{13/2}$. Another blue emission band at 488 nm corresponds to the $^4F_{9/2} \rightarrow {}^6H_{15/2}$ transition, [6] which is less sensitive to the host. The excitation spectrum of Dy^{3+} doped Y_2O_2S was recorded keeping the emission wavelength at 575 nm. The spectra consists of several excitation bands of the f-f transitions, which are ascribed to the different transitions from the ground state $^6H_{15/2}$ to the various excited states of the $4f^9$ electronic configuration of the Dy^{3+} ions. The excitation maxima located at 351 nm corresponds to the hypersensitive transition from the ground $^6H_{15/2}$ to $^6P_{7/2}$ level. This excitation spectrum matches well with that of the NUV-light.[6, 12] It is hence suggested that this phosphor is suitable for solid state lighting. When the Dy^{3+} concentration was varied from 1 mol% to 5 mol%, the emission intensity first increased up to 3 mol% and then decreased concluding that the optimum doping concentration of Dy^{3+} in the Y_2O_2S host is 3 mol% (Fig. 5 (d)). Beyond this optimum concentration, the intensity decreases due to the concentration quenching phenomena resulting from resonance energy transfer between neighbouring Dy^{3+} ions.[6] The relative intensity ratio between the electric dipole transition and the magnetic dipole transition is known as an asymmetric ratio that is the measure of the structural distortion around the Dy^{3+} ions. The calculated asymmetric ratios for the various concentrations of the Dy^{3+} doped Y_2O_2S phosphors are found to be 1.57, 1.59, 1.60, 1.58 and 1.57 respectively.[12] This value is greater than 1 indicates that the surroundings of Dy^{3+} ion is distorted.

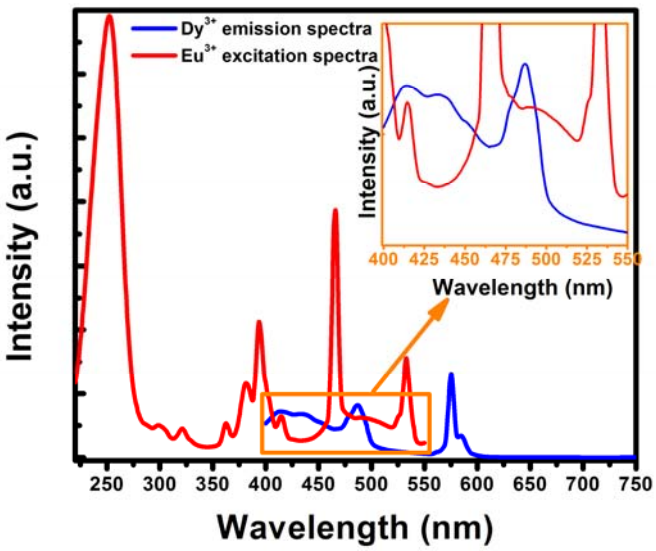

Fig. 6: *Spectral overlap between PL spectra of Y_2O_2S: Dy^{3+} and PLE spectra of Y_2O_2S: Eu^{3+}phosphors*

As shown in Fig. 5 (a and c) and Fig. 6, the comparison of the PLE and PL spectra for Y_2O_2S: Eu^{3+} and Y_2O_2S: Dy^{3+} phosphors reveal a significant spectral overlap between the excitation band of Eu^{3+} and the Dy^{3+} emission transitions. Therefore, the effective energy transfer from Dy^{3+} to Eu^{3+} is expected.[36] This type of energy transfer is quite common and has been observed in several Eu^{3+} and Dy^{3+} co-activated phosphors such as in silicate glass [37] and fluoride materials.[12] Moreover, the Eu^{3+} or Dy^{3+} solely doped Y_2O_2S emits red, blue or yellow light, so it is possible to obtain white-light emission by tailoring the red, blue or yellow light in Eu^{3+} and Dy^{3+} co-doped Y_2O_2S phosphor varying the Dy^{3+}/ Eu^{3+} doping concentration.

Effect of codoping and energy transfer. Fig. 7 (a-b) shows the emission spectra of the Y_2O_2S: Eu^{3+}, Dy^{3+} phosphors as a function of the Eu^{3+} concentration with a fixed Dy^{3+} concentration of 3 mol % and Dy^{3+} concentration with a fixed Eu^{3+} concentration of 5 mol %, respectively. Fig. 7(a) shows the emission spectra of the Eu^{3+}, Dy^{3+}co-doped phosphors taking different mass ratios of Dy^{3+}/ Eu^{3+} = 3:0, 3:1, 3:2, 3:3, 3:4, 3:5. The corresponding

integrated PL intensity of the Eu^{3+} activator (or energy acceptor) was observed to increase, whereas that of Dy^{3+} sensitizer (or energy donor) is simultaneously found to decrease monotonically with increasing the Eu^{3+} dopant content. On the other hand, by taking different mass ratios of Eu^{3+}/ Dy^{3+} = 5:0, 5:1, 5:2, 5:3, 5:4, 5:5 (Fig. 7(b)) both the Eu^{3+} and Dy^{3+} characteristics peaks decreased. These above two phenomena indicate that the Eu^{3+} emission is enforced by the introduction of Dy^{3+} and this is attributed to the energy transfer phenomena from Dy^{3+} ion to Eu^{3+} ion in the Y_2O_2S host material. Here, Eu^{3+} acts as an activator and Dy^{3+} as a sensitizer.[20] Fig. 7(c) shows the energy level scheme of Eu^{3+} and Dy^{3+} ions in the Y_2O_2S host and the schematic energy transfer mechanism between Dy^{3+} and Eu^{3+} ions.

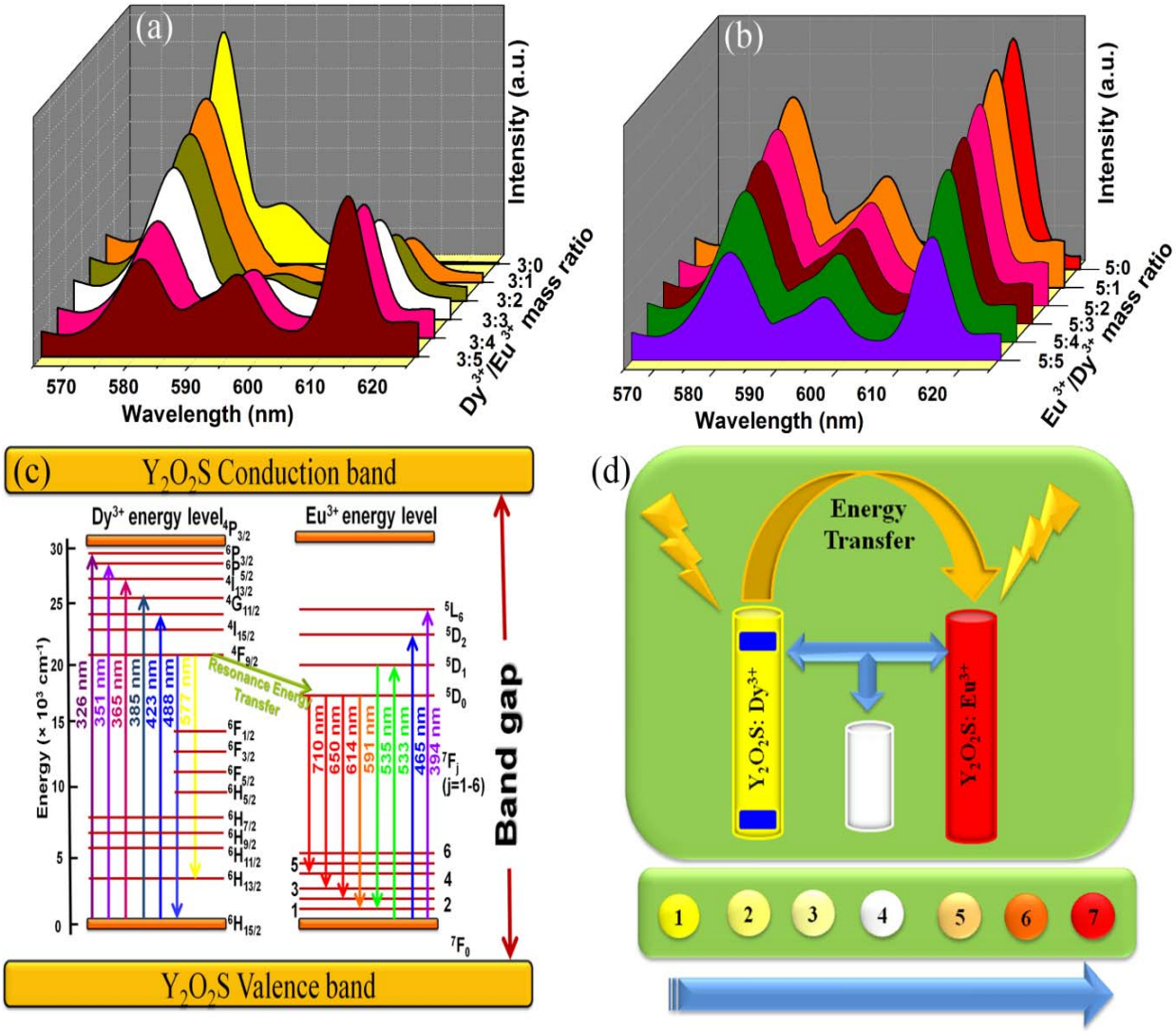

Fig.7: *(a-b) Emission spectra of Y_2O_2S co-doped with various mass ratio of Eu^{3+} to Dy^{3+} (c) Energy transfer scheme from Dy^{3+} to Eu^{3+} (d) Schematic representation of energy transfer*

Thus, white-light can be obtained by combining the blue-yellow emission of the Dy^{3+} ions and red emission of the Eu^{3+} ions in a single host lattice with properly tuning the relative ratio of the Eu^{3+} to Dy^{3+} ions through the principle of energy transfer.

To further identify the evidence of energy transfer from the Dy^{3+} to Eu^{3+} ions, the PL decay curves of the Dy^{3+} ions in Y_2O_2S: Eu^{3+}, Dy^{3+} were measured with an excitation at 285 nm and monitored at 575 nm, as represented in Fig. 8 (a). The decay curve for singly Dy^{3+}-doped Y_2O_2S can be well fitted into the bi exponential function as

$$I = y_0 + A_1 \exp(-t/\tau_1) + A_2 \exp(-t/\tau_2) \quad (6)$$

where τ_1 (fast components) and τ_2 (slow components) are attenuation times which determines the decay rate for corresponding exponential components, A_1 and A_2 are fitting parameters. The average life times were calculated using the formula[38]

$$\langle \tau \rangle = (A_1\tau_1^2 + A_2\tau_2^2)/(A_1\tau_1 + A_2\tau_2) \quad (7)$$

On the basis of this equation and decay curves, the lifetime values were determined to be 11.8, 10.6, 8.9, 7.8, 6.6 and 5.8 s for y = 0. 0.01. 0.02, 0.03, 0.04 and 0.05 in $Y_{1.97-y}Eu_yDy_{0.03}O_2S$, respectively.

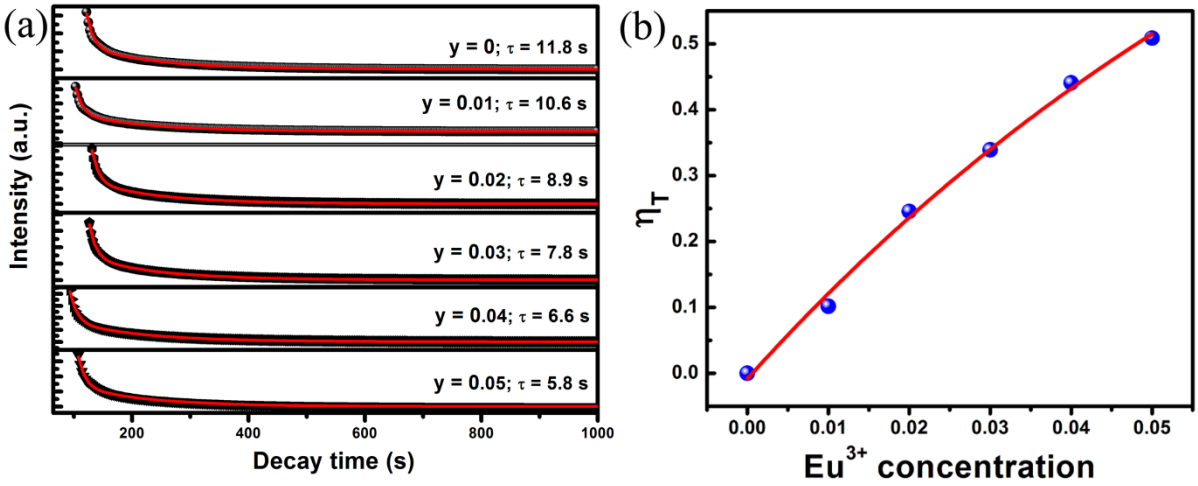

Fig.8: *(a) PL decay curve of Dy^{3+}, in $Y_2O_2S:Eu^{3+}/Dy^{3+}$ phosphor and (b) Dependence of energy transfer efficiency in $Y_2O_2S:Eu^{3}$, Dy^{3+} on the content of Eu^{3+}.*

The doping of Eu^{3+} ions significantly modifies the fluorescent dynamics of the Dy^{3+} ions. The decay lifetime for Dy^{3+} was found to reduce with increasing Eu^{3+} doping content, which strongly demonstrated the energy transfer from Dy^{3+} to Eu^{3+}, as reported by Ruelle et al. [39] and Jia et al. [40] respectively. These results give further evidence that the transfer process happen through a resonance-type energy transfer mechanism.[36] We are also interested in investigating the energy transfer efficiency (η_T) of $Dy^{3+} \rightarrow Eu^{3+}$ and a simple operational definition as suggested by Paulose et al., [41] η_T can be expressed by

$$\eta_T = 1 - \frac{\tau_S}{\tau_{SO}} \qquad (8)$$

where τ_{S0} is the intrinsic decay lifetime of the sensitizer (Dy^{3+}) and τ_S is the decay lifetime of the sensitizer (Dy^{3+}) in the presence of the activator (Eu^{3+}). The η_T for $Dy^{3+} \rightarrow Eu^{3+}$ in $Y_2O_2S:Eu^{3+}$, Dy^{3+} was calculated and is illustrated in Fig. 8(b) as a function of Eu^{3+} concentration. The η_T was found to increase gradually from y = 0 to 0.05 with the increase of Eu^{3+} content in $Y_{1.97-y}Eu_yDy_{0.03}O_2S$.

Forster defined the energy transfer efficiency (η_T) in terms of fluorescence intensities in the presence and absence of acceptors as: [20]

$$\eta_T = 1 - \frac{\eta}{\eta_0} = 1 - \frac{I}{I_0} \quad (9)$$

The calculated transfer efficiencies are summarized in Table 1. There is a good agreement between energy transfer efficiencies obtained from the decay time data and that determined from emission spectra. This good agreement suggests that the $Dy^{3+} \rightarrow Eu^{3+}$ energy transfer through a radiative mechanism is neglected, since radiative energy transfer does not cause any reduction in the sensitizer decay time.

This transfer of energy may occur via one of the following mechanisms: exchange interaction or multipole–multipole interaction.[42-43] The type of the interaction mechanism can be identified by knowing the critical distance (R_c) between the donor and acceptor rare earth ions. If the R_c is greater than 5 Å, then multipolar interaction dominates and if R_c is lesser than 5 Å, exchange interaction will be the main mechanism for energy transfer. As suggested by Blasse, [44] the average separation $R_{Dy\text{-}Eu}$ can be expressed by

$$R_{Dy-Eu} \approx 2\left[\frac{3V}{4\pi\chi N}\right]^{1/3} \quad (10)$$

where N is the number of ions in the unit cell, V is the volume of the unit cell and χ is the total concentration of Eu^{3+} and Dy^{3+}. For the Y_2O_2S host, $N = 5$ and $V = 97.44$ Å^3. Thus, $R_{Dy\text{-}Eu}$ (in Å) is determined to be 9.8, 9.1, 8.6, 8.2, and 7.9 Å for y = 0.01, 0.02, 0.03, 0.04, and 0.05, respectively, in $Y_{1.97-y}Eu_yDy_{0.03}O_2S$. The critical concentration (χ_c), at which the luminescence intensity of Dy^{3+} is half of that sample in the absence of Eu^{3+}, is 0.048. This is clearly shown in the dependence of the relative emission intensity of Dy^{3+} on different Eu^{3+} dopant content and is represented in Fig. 9 (a). Therefore, the critical distance (R_c) of energy

transfer was calculated to be about 9.4 Å which indicates that the multipole–multipole interaction is dominant and which is the major cause for energy transfer in the present case. It was also observed that the radiative emission from Dy^{3+} prevails when $R_{Dy\text{-}Eu} >> R_c$ and energy transfer from Dy^{3+} to Eu^{3+} dominates when $R_{Dy\text{-}Eu} < R_c$.[7, 36]

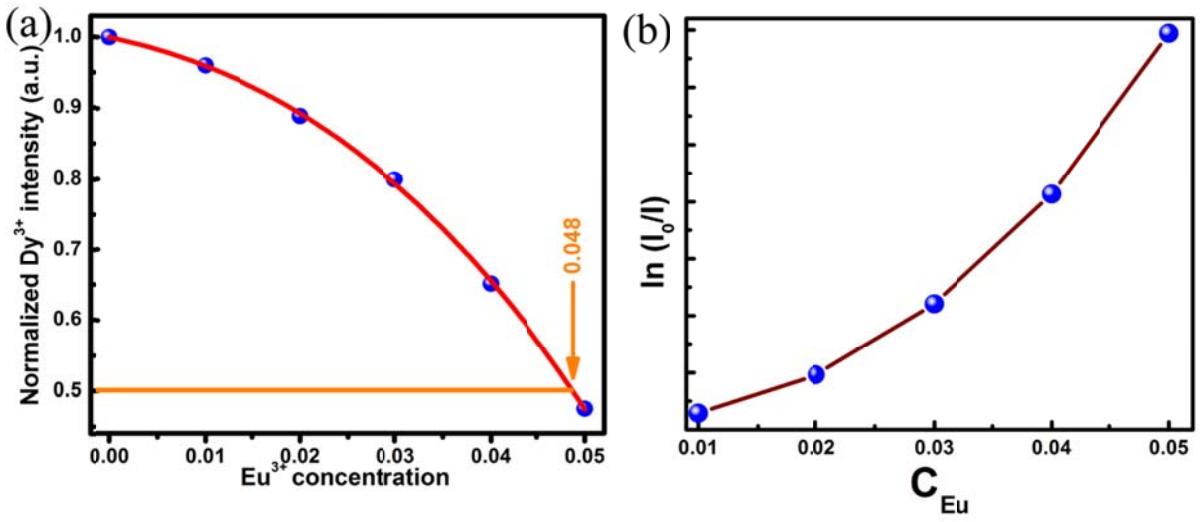

Fig.9: *(a) Dependence of relative Dy^{3+} emission intensity in $Y_2O_2S:Eu^{3+}$/ Dy^{3+} on the content of Eu^{3+} and (b) The dependence of ln (I_0/I) of Dy^{3+} on C_{Eu}.*

Another way to determine the main cause in a further deeper way for energy transfer phenomena is described below. On the basis of the Dexter's energy transfer expressions of exchange interaction, the following relation can be given as [45]

$$\ln(\frac{I_0}{I}) \propto C \qquad (11)$$

where I_0 is the intrinsic luminescence intensity of the Dy^{3+} ions and I is the luminescence intensity of the Dy^{3+} ions with the activator (Eu^{3+}) present; C is the doping concentration of the Eu^{3+} ions. The ln(I_0/I)–C plot shows a non-linear relationship (Fig. 9 (b)), indicating that the exchange interaction is not a dominant energy transfer mechanism in Y_2O_2S: Eu^{3+}, Dy^{3+}.

Based on Dexter's energy transfer formula of multipolar interactions and Reisfeld's approximation, the following relation can be obtained: [46]

$$\frac{\eta_0}{\eta} \approx \frac{I_0}{I} \propto C^{n/3} \quad (12)$$

where η_0 and η are the luminescence quantum efficiencies of donor in the absence and presence of acceptor, respectively and C is the sum of donor and acceptor ions concentrations. n = 6, 8 and 10, corresponds to dipole–dipole, dipole–quadrupole, and quadrupole–quadrupole interactions, respectively.[17] The values ($\frac{\eta_0}{\eta}$) can be found from the ratio of I_0/I where I_0 and I are the fluorescence intensities of donor in the absence and presence of acceptor, respectively. The I_0/I–$C^{n/3}$ plots are further illustrated in Fig. 10 (a–c), and the relationship is observed when n = 6, 8, and 10. A linear relation was observed when n = 8. This clearly indicates that the energy transfer mechanism from the Dy^{3+} to Eu^{3+} ions is a dipole–quadrupole reaction. Therefore, the electric dipole–quadrupole interaction predominates in the energy transfer mechanism from the Dy^{3+} to Eu^{3+} ions in $Y_2O_2S:Eu^{3+}$, Dy^{3+}.[7, 36]

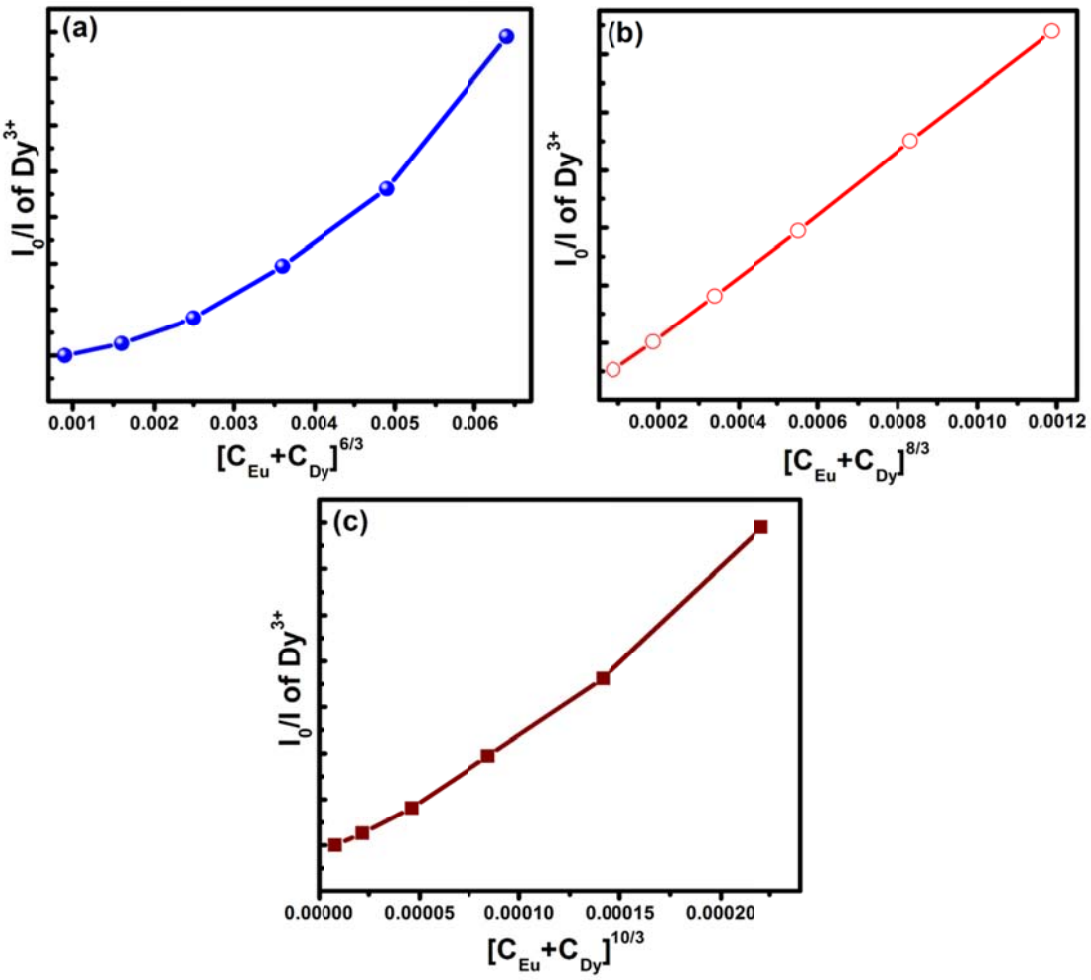

Fig.10: *The dependence of I_0/I of Dy^{3+} on (a) $C^{6/3}$, (b) $C^{8/3}$ and (c) $C^{10/3}$*

Considering the dipole-quadrupole interaction, the energy transfer probability P_{SA} (in s^{-1}) from a sensitizer to an accepter is given by the following formula of Dexter[7, 36]

$$P_{Dy-Eu} = 3.024\times10^{12}\frac{\lambda_S^2 f_q}{R^8\tau_S}\int\frac{F_S(E)F_A(E)dE}{E^4} \qquad (13)$$

where f_q is the oscillator strength of the involved absorption transition of the acceptor (Eu^{3+}), λ_S (in Å) is the wavelength position of the sensitizer's emission, τ_S is the radiative decay time of the sensitizer (in seconds), R is the sensitizer–acceptor average distance (in Å), E is the energy involved in the transfer (in eV), and $\int F_S(E)F_A(E)/E^4dE$ represents the spectral

overlap between the normalized shapes of the Dy^{3+} emission $F_S(E)$ and the Eu^{3+} excitation $F_A(E)$, and in our case it is calculated to be about 0.01565 eV^{-5}. The critical distance (R_C) of energy transfer from the sensitizer to the acceptor is defined as the distance for which the probability of transfer equals the probability of radiative emission of donor, the distance for which $P^{DQ}\tau_s = 1$. Hence, R_C can be obtained from Eq. 13 as[7, 36, 47]

$$R_C^8 = 3.024\times10^{12}\,\lambda_S^2 f_q \int \frac{F_S(E)F_A(E)dE}{E^4} \qquad (14)$$

In the wavelength region of Dy^{3+} emission (400–600 nm) the f_d electric dipole oscillator strength of the Eu^{3+} is very low (1.2×10^{-8})[46], since the Eu^{3+} transition is more or less forbidden as an electric dipole transition by the parity selection rule.[48] The f_q electric quadrupole oscillator strength was estimated from its relation with f_d, $f_q = (a/\lambda_a)^2 f_d$.[1] Using a ≈ 1 Å (radius of the Eu^{3+}) and $\lambda_{Eu} \approx 4880$ Å (wavelength of the absorbed light by the europium in the dysprosium emission), and considering that the forbidden electric dipole transitions are weaker than the allowed ones by a factor of 10^{-4} to 10^{-5}, then the ratio f_q/f_d is 4.2×10^{-3} for the Eu^{3+}.[1] So, the oscillator strength of the Eu^{3+} electric quadrupole transition (f_q) is about 5.04×10^{-11}.[49] From the above equation, on the basis of these values and the calculated spectral overlap, the critical distance R_c was estimated to be 9.3 Å. This result is in good agreement with that obtained using the concentration quenching method. Using eqn. 13 and 14, the probability of energy transfer can be rewritten as,

$$P_{Dy-Eu} = \frac{1}{\tau_s}\left(\frac{R_c}{R}\right)^8 \qquad (15)$$

and it is summarized in Table 1.

Table 1 Energy transfer efficiency, average donor-acceptor distances and probability of energy transfer.

C_{donor} (mol %)	$C_{acceptor}$ (mol %)	R_{Dy-Eu} (Å)	I_0	I	η / η_0	η_T (%)		P_{Dy-Eu} (s^{-1})
						From emission	From Decay kinetics	
3	0	-	134	-	1	-	-	-
	1	9.8	-	118	0.88	12	11	68
	2	9.1	-	98	0.73	27	25	150
	3	8.6	-	87	0.65	35	33	260
	4	8.2	-	74	0.55	45	42	450
	5	7.9	-	64	0.48	52	49	692

Photometric Characterization. Fig. 11 illustrates the CIE (International Commission on Illumination) chromaticity diagram of $Y_2O_2S:Eu^3$, Dy^{3+} phosphors for different Dy^{3+} / Eu^{3+} mass ratios. CIE parameters such as colour coordinates (x, y) and colour correlated temperature (CCT) were calculated to characterize the colour emission.[7] The colour coordinates were determined using the Colour calculator software. The colour correlated temperature (CCT) is given by the McCamy empirical formula[50]

$$CCT = - 437n^3 + 3601n^2 - 6861n + 5514.31 \quad (15)$$

where $n = (x-x_e) / (y-y_e)$ and chromaticity epicentre is at $x_e = 0.3320$ and $y_e = 0.1858$.[6]

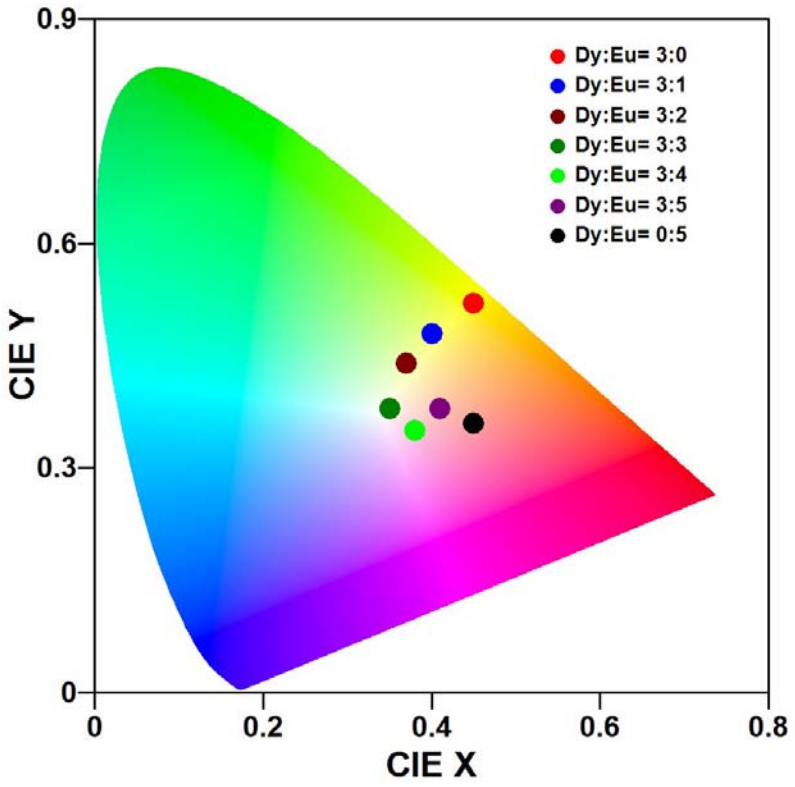

Fig.11: Variation of c*olour co-ordinate with* Dy^{3+}*/* Eu^{3+} *mass ratio in* $Y_2O_2S:Eu^{3+}/ Dy^{3+}$

From the chromaticity diagram (Fig. 11), it can be seen that the colour coordinates traverses a wide range from the yellow to the red region on varying the Dy^{3+}/ Eu^{3+} mass ratios. The results show that the tuning of the emission colour is possible by the change of the Dy^{3+}/ Eu^{3+} mass ratios. A near white light was achieved for 3 mol% Dy^{3+}/Eu^{3+} concentration with colour coordinates (0.34, 0.32). This colour coordinate is close to the standard D65 daylight with coordinates of 0.3129 (x)/0.3292 (y).[51] The CCT value of the studied phosphors were found to vary from 1871 – 6125 K. Generally, CCT value greater than 5000 K indicates the cold white light used for commercial lighting purpose. The obtained CCT value (6125 K) for the near white light emitting phosphor agrees with the CCT value of standard daylight at noon (D65, 6500 K) suitable for cold near white light emission.[52-54] These results of the 3 mol% Dy^{3+}/ Eu^{3+} co-activated Y_2O_2S phosphor are in good agreement with the photometric parameter data reported elsewhere[51-54] and support the application of this phosphor as a cold

near white light source for solid state lighting. The values of the CIE parameters for the different co-doped phosphors are summarized in Table 2.

Table 2 CIE parameters of $Y_2O_2S:Eu^{3+}/ Dy^{3+}$ with different Eu^{3+} and Dy^{3+} doping ration

$(Y_{2-x-y}Eu_xDy_{y)2}O_2S$ x:y	Colour Coordinates		CCT (K)
3:0	0.45	0.52	3600
3:1	0.42	0.48	3972
3:2	0.37	0.44	4597
3:3	0.34	0.32	6125
3:4	0.38	0.30	3294
3:5	0.41	0.32	2657
0:3	0.45	0.31	1871

CONCLUSIONS

A series of Eu^{3+} and Dy^{3+} co-activated Y_2O_2S phosphors were synthesized by the hydrothermal route and the luminescence properties were investigated under photo-excitation. The obtained phosphor exhibits a broad excitation band ranging from 250 to 500 nm, which can perfectly match a near- UV light indicating the suitability of these materials for lighting technology. The spectroscopic data indicate that the $Dy^{3+} \rightarrow Eu^{3+}$ energy transfer process takes place in the host matrix of Y_2O_2S. The non-radiative character of this transfer is inferred from both a decrease of the Dy^{3+} overall emission and a decrease in the decay rate of the Dy^{3+} emission, when the phosphor is co-doped with dysprosium and europium. From spectroscopic data, it is inferred that Dy^{3+} to Eu^{3+} energy transfer via an electric dipole–quadrupole interaction appears to be the most probable energy transfer mechanism. The efficiency of this transfer is enhanced up to 52% for the phosphors with the highest Eu^{3+} content. The critical energy transfer distance has also been calculated by the concentration quenching and spectral overlap methods. The results obtained from the two approaches are in good agreement. Furthermore, it was also demonstrated that the $Y_{2-x-y}O_2S: Eu_x^{3+}$, Dy_y^{3+} can

be systematically tuned to generate white light under ultraviolet radiation and it has been shown to exhibit the potentiality to act as a single-emitting-component white-emitting phosphor for solid state lighting applications.

ACKNOWLEDGMENT

The authors are thankful to University Grants Commission, New Delhi, Government of India for funding this work under Special Assistance Programme (No.F. 530/1/DRS/2009 (SAP-I)). The research is also supported by the South African Research Chairs Initiative of the Department of Science and Technology and National Research Foundation of South Africa. The financial support from the Cluster program of the University of the Free State is highly recognized.

REFERENCES

(1) R. Martínez-Martínez, S. Rivera, E. Yescas-Mendoza, E. Álvarez, C. Falcony and U. Caldiño, *Opt. Mater.* **2011**, *33*, 1320.

(2) M. Jiao, N. Guo, W. Lu, Y. Jia, W. Lv, Q. Zhao, B. Shao and H. You, *Inorg. Chem.* **2013**, *52*, 10340.

(3) S. Som, S. Dutta, V. Kumar, V. Kumar, H. C. Swart and S. K. Sharma, *J. Lumin.* **2014**, *146*, 162.

(4) H. Li, H. M. Noh, B. K. Moon, B. C. Choi, J. H. Jeong, K. Jang, H. S. Lee and S. S. Yi, *Inorg. Chem.* **2013**, *52*, 11210.

(5) X. Jin, M. Götz, S. Wille, Y. K. Mishra, R. Adelung and C. Zollfrank, *Adv. Mater.* **2013**, *25*, 1342.

(6) S. Dutta, S. Som and S. K. Sharma, *Dalton Trans.* **2013**, *42*, 9654.

(7) N. Guo, H. You, Y. Song, M. Yang, K. Liu, Y. Zheng, Y. Huanga and H. Zhang, *J. Mater. Chem.* **2010**, *20*, 9061.

(8) W. Lu, N. Guo, Y. Jia, Q. Zhao, W. Lv, M. Jiao, B. Shao and H. You, *Inorg. Chem.* **2013**, *52*, 3007.

(9) B. Liu, C. Shi and Z. Qi, *Appl. Phys. Lett.* **2005**, *86*, 191111.

(10) Z. Xia, J. Zhuang and L. Liao, *Inorg. Chem.* **2012**, *51*, 7202.

(11) S. Som, S. K. Sharma and T. Shripathi, *J. Fluoresc.* **2013**, *23*, 439.

(12) V. R. Bandi, B. K. Grandhe, H.-J.Woo, K. Janga, D. S. Shin, S.-S. Yi and J.-H. Jeong, *J. Alloys Compd.* **2012**, *538*, 85.

(13) P.-F. Ai, Y.-L. Liu, L.-Y. Xiao, H.-J. Wang and J.-X. Meng, *Sci. Technol. Adv. Mater.* **2010**, *11*, 035002 (5pp).

(14) O. Y. Manashirov, A. N. Georgobiani, V. B. Gutan, E. M. Zvereva and A. N. Lobanov *Inorg. Mater.* **2012**, 48, 721.

(15) L. Lin, C. Kun, W. Zhifang, Y. Baogui, C. Yonghu, Z. Weiping and S. Chaoshu, *J. Rare Earth.* **2008**, *26*, 648.

(16) C. Cui, G. Jiang, P. Huang, L. Wang and D. Liu, *J. Lumin.* **2014**, *145*, 665.

(17) E.-J. Popovici, L. Muresan, H.-S. Amalia, E. Indrea, M. Vasilescu, M. Nazarov and J. D. Young, *Opt Mater.* **2004**, *27* 559.

(18) S. Som, A. Choubey and S. K. Sharma, *J. Exp. Nanosci.* **2013**, doi: 10.1080/17458080.2013.837972.

(19) X. Zhou, M. Xing, T. Jiang, Y. Fu, Y. Peng, H. Wang and H. Luo, *J. Alloys Compd.* **2014**, doi: 10.1016/j.jallcom.2013.09.155.

(20) S. Som and S. K. Sharma, *J. Phys. D: Appl. Phys.* **2012**, 45, 4151021.

(21) Y. K. Mishra, S. Kaps, A. Schuchardt, I. Paulowicz, X. Jin, D. Gedamu, S. Freitag, M. Claus, S. Wille, A. Kovalev,S. N. Gorb and R. Adelung, *Part. Part. Syst. Charact.* **2013**, 30, 775.

(22) R. L. Frost, Y. Xi, R. Scholz, F. M. Belotti and M. Beganovic, *Spectrochim. Acta* A, **2013**, 110, 7.

(23) V. Kumar, N. Singh, V. Kumar, L. P. Purohit, A. Kapoor, O. M. Ntwaeaborwa and H. C. Swart, *J Appl. Phys.* **2013**, 114, 134506.

(24) S. Jebril, H. Kuhlmann, S. Muller, C. Ronning, L. Kienle, V. Duppel, Y. K. Mishra and R. Adelung, *Cryst. Growth Des.* **2010**, *28*, 42

(25) S. Som, S. K. Sharma and S. P. Lochab, Phys. Status Solidi A, **2013**, 210, 1624.

(26) X. Jin, J. Strueben, L. Heepe, A. Kovalev, Y. K. Mishra,R. Adelung, S. N. Gorb and Anne Staubitz, *Adv. Mater.* **2012**, *24*, 5676.

(27) G. Q. Zhang and X. W. D. Lou, *Sci. Rep.* **2013**, *3*, 1470.

(28) M. Ye, H. Zhong, W. Zheng, R. Li and Y. Li, *Langmuir* **2007,** *23,* 9064.

(29) R. Li, X. Tao and X. Li, *J. Mater. Chem.* **2009**, *19*, 983.

(30) S. Som, S. K. Sharma and S. P. Lochab, *Mater. Res. Bull.* **2013**, *48*, 844.

(31) A. E. Morales, E. S. Mora and U. Pal, *Rev. Mex. Fis. S* **2007**, *53(5)* 18.

(32) S. Dutta, S. Som, J. Priya and S. K. Sharma, *Solid State Sci.* **2013**, *18*, 114.

(33) J. Tauc and A. Menth, *J. Non-crystal Solids* **1972**, *8*, 569.

(34) C. Guo, L. Luan, C. Chen, D. Huang, Q. Su, *Mater. Lett.* **2008**, *62*, 600.

(35) S. Som, A. Choubey and S. K. Sharma, *Physica B* **2012**, *407*, 3515.

(36) W.-J. Yang, L. Luo, T.-M. Chen and N.-S. Wang, *Chem. Mater.* **2005**, *17*, 3883.

(37) X.-Y. Sun, M. Gu, S.-M. Huang, X.-L. Liu, B. Liu and C. Ni, *Physica B* **2009**, *404*, 111.

(38) C.-H. Huang and T.-M. Chen, *Opt. Express* **2010**, *18*, 5089.

(39) N. Ruelle, M. Pham-Thi and C. Fouassier, *Jpn. J. Appl. Phys.* **1992**, *31*, 2786.

(40) C. Jia-li, L. Ruo-ying, Z. Chong-jian, T. Shao-long, X. Wan and S. Jun-ying, *Opt. Mater.* **2012**, *34*, 1112.

(41) P. I. Paulose, G. Jose, V. Thomas, N. V. Unnikrishnan, M. K. R. Warrier, *J. Phys. Chem. Solids* **2003**, *64*, 841

(42) G. Blasse and B. C. Grabmarier, *Luminescent Materials*; Sprinnger- Verlag: Berlin, Germany, **1994**, 96.

(43) R. Reisfeld and N. Lieblich-sofer, *J. Solid State Chem.* **1979**, *28*, 391.

(44) G. Blasse, *Philips. Res. Rep.* **1969**, *24*, 131.

(45) D. L. Dexter and *J. Chem. Phys.* **1953**, *21*, 836.

(46) D. L. Dexter and J. A. Schulman, *J. Chem. Phys.* **1954**, *22*, 1063.

(47) Y. Zhang, G. Li, D. Geng, M. Shang, C. Peng and J. Lin, *Inorg. Chem.* **2012**, *51*, 11655.

(48) I. M. Batyaev and S. M. Shilov, *J. Appl. Spectrosc.* **1984**, *41*, 815.

(49) R. Martinez-Martinez, A. C. Lira, A. Speghini, C. Falcony, U. Caldino, *J. Alloys Compd.* **2011**, *509*, 3160.

(50) C. S. McCamy, *Color Res. Appl.* **1992**, *17*, 142.

(51) C. Lorbeer and A. V. Mudring, *J. Phys. Chem. C* **2013**, *117*, 12229.

(52) http://www.hunterlab.com/appnotes/an05_05.pdf

(53) S. H. Lee, J. H. Park, S. M. Son and J. S. Kim, *Appl. Phys. Lett.* **2006**, *89*, 221916.

(54) T. W. Murphy Jr, *J. Appl. Phys.* **2012**, *111*, 1049091.

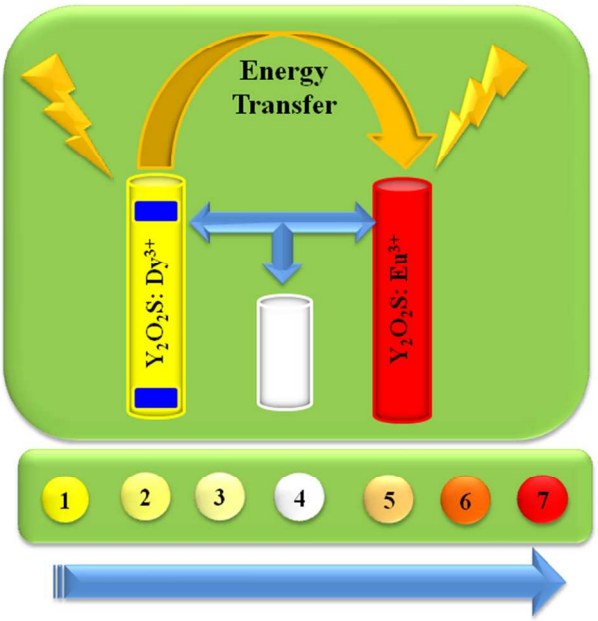

254x190mm (96 x 96 DPI)